The Development of Negative Moist Potential Vorticity in the Stratiform Region of a Simulated Squall Line

DA-LIN ZHANG

Department of Atmospheric and Oceanic Services, McGill University, Montreal, Quebec, Canada

HAN-RU CHO

Department of Physics, University of Toronto, Toronto, Ontario, Canada

(Manuscript received 17 April 1991, in final form 30 September 1991)

ABSTRACT

This paper presents evidence on the development of negative moist potential vorticity (MPV) or moist symmetric instability (MSI) in the stratiform region of a midlatitude squall line, based on a three-dimensional (3D) numerical simulation of a case that occurred on 10–11 June 1985 during the Preliminary Regional Experiment for STORM-Central (PRE-STORM). The results show that the stratiform region, though convectively stable to pure vertical displacement, is considerably unstable to slantwise displacement along the system's broad front-to-rear (FTR) saturated ascending flow. It is found that this instability evolves from boundary-layer convective instability that has previously been removed by upright convection over the leading portion of the squall system. The negative MPV in the stratiform region is mainly the result of upward and rearward transport of the low-level convectively unstable air along the sloping FTR ascending flow and of processes that reverse the signs of both the convective stability parameter (i.e., $\partial\theta_e/\partial z$) and the absolute vorticity (i.e., $\partial v/\partial n - \partial u/\partial s + f$). The resulting symmetric instability appears to considerably enhance the vertical motion and precipitation rate in the stratiform clouds. In the stratiform region of the squall system, the negative MPV leads to a region of negative absolute vorticity or inertial instability at the upper levels, and it may be responsible for the strong anticyclonic divergent outflow in that region. Thus, the effect of the squall system is to process the low-level negative MPV in such a way as to symmetrically stabilize the lower troposphere and inertially destabilize the upper troposphere. The roles of convective, symmetric, and inertial instabilities in the development of the squall system and their implications with respect to intense oceanic storms are discussed.

1. Introduction

In recent years, progress toward understanding the development of mesoscale convective systems (MCS's) has accelerated primarily due to advances in computational facilities and large field experiments such as the Global Atmospheric Research Program (GARP) Atlantic Tropical Experiment (GATE) (see Kuettner and Parker 1976) and the Preliminary Regional Experiment for STORM-Central (PRE-STORM) (see Cunning 1986). One of the most important findings is related to the broad region of trailing stratiform precipitation that occurs in both tropical and midlatitude squall lines (Zipser 1969, 1977; Houze et al. 1989, 1990). Specifically, the trailing stratiform precipitation has been found to account for as much as 40% of the total rainfall of this type of squall system (Houze 1977; Churchill and Houze 1984; Johnson and Hamilton 1988), and it also seems to be correlated to the appearance and intensification of some mesovortices or mesoscale convective complexes (MCCs) (Smull and Houze 1985; Leary and Rappaport 1987; Zhang and Fritsch 1987, 1988b). Associated with this type of squall system are often intense convective-scale updrafts along the leading line, pronounced front-to-rear (FTR) ascending currents within the broad stratiform region, and significant rear-to-front (RTF) descending flow below the stratiform cloud base (Ogura and Liou 1980; Johnson and Hamilton 1988; Zhang and Gao 1989).

The large amount of stratiform precipitation has received considerable attention with regard to the origins of precipitable water and the effects of diabatic heating on the airflow in the vicinity of squall systems. In earlier studies, the formation of trailing stratiform clouds has been viewed as a consequence of the propagation of deep convective cells relative to the gust front. Thus, the leading convective line tends to leave in its wake a series of cloud towers and anvils in various stages of decay, known as the "old towers" hypothesis (e.g., Newton 1950; Pedgley 1962; Zipser 1969, 1977; Houze 1977; Zipser et al. 1982). In a recent study, Smull and Houze (1985) examined the water budgets

Corresponding author address: Dr. Da-Lin Zhang, Department of Atmospheric and Oceanic Sciences, McGill University, 805 Sherbrooke St. West, Montreal H3A 2K6, Quebec, Canada.

of a midlatitude squall line and found that hydrometeors falling from the upper portions of the leading convective cells can be spread over a mesoscale distance rearward by the strong relative FTR flow. Hence, they hypothesized that most of the trailing stratiform precipitation could be produced by the fallout of the rearwardly advected ice particles from the leading convective line. Later, using a two-dimensional diagnostic model, Rutledge and Houze (1987) validated the Smull–Houze hypothesis, although their results appear to be sensitive to the magnitude of the FTR flow and the vertical distribution of hydrometeors.

While the aforementioned kinematic interpretations have provided certain insights into the development of trailing stratiform precipitation, little is understood about the actual dynamics taking place in the stratiform region. In particular, this large amount of stratiform rainfall develops under a convectively (or potentially) stable[1] environment (i.e., the equivalent potential temperature θ_e increases with height). However, updrafts as strong as 1 m s^{-1} have often been observed in this trailing stratiform region (Ogura and Liou 1980; Rutledge et al. 1988). This magnitude is one to two orders larger than what can possibly be attained in baroclinically driven weather systems. Therefore, a natural question is: How could such strong upward motion and significant amount of rainfall be developed under a convectively stable condition? There are some plausible explanations for the phenomena, such as 1) the presence of dying convective cells whose updrafts still have upward momentum, and 2) the destabilization of the stratiform region due to radiative processes. However, in this paper we shall provide some evidence that suggests a different mechanism for the development of stratiform precipitation with strong upward motion.

For this study, we use moist potential vorticity (MPV) as a fundamental dynamical variable to examine a four-dimensional dataset obtained from an 18-h high-resolution (Δx = 25 km) simulation of a squall line that occurred during 1200 UTC 10 June–0600 UTC 11 June 1985 in PRE-STORM (see Zhang et al. 1989; Zhang and Gao 1989). The results reveal that the stratiform region is characterized by negative MPV and suggest that trailing stratiform precipitation could be viewed as an end product of slantwise convection with pronounced moist symmetric instability (MSI). To our knowledge, this concept has not been addressed before. Thus, it is the purpose of this paper to provide evidence that suggests the presence of MSI associated with the squall stratiform precipitation. The presentation of the paper is organized as follows. Section 2 provides the basic background, including the description of meteorological conditions and model simulation associated with the squall system, and it also describes the methodology used for this study. Section 3 shows evidence of negative MPV in the stratiform region of the simulated squall line, whereas section 4 presents the structure and evolution of the negative MPV in relation to the squall circulation. Discussion and concluding remarks are given in the final section.

2. Background and methodology

The squall line under investigation was initiated at 2100 UTC or 1500 LST 10 June 1985 (see Fig. 1a) as a weak surface front moved toward the PRE-STORM network and interacted with a thermal boundary (see Johnson and Hamilton 1988; Zhang et al. 1989). Then, it intensified rapidly in response to a widespread convectively unstable environment over the network and advanced southeastward at a speed of 14–16 m s^{-1} (see Fig. 1b). Associated with the intensification was the development of a mesovortex to the northeast of the system. During this stage, both the satellite imagery and radar echoes display rapid expansion of stratiform clouds behind the leading convective line, particularly over the portion where the mesovortex was located (see Figs. 1b–d). Water-budget calculations by Johnson and Hamilton (1988) indicate a significant contribution (30%–40%) of stratiform rainfall to the total squall precipitation. The squall system reached nearly a steady state during the mature stage around 0300 UTC 11 June. During this stage, the leading line was 50–70 km wide and was followed by a region of stratiform precipitation that was roughly 150 km wide (see Fig. 1d).

For the numerical simulation, an improved nested-grid version of the Pennsylvania State University–National Center for Atmospheric Research (NCAR) Mesoscale Model (Anthes et al. 1987) was used in which a modified version of the Fritsch–Chappell (1980) cumulus parameterization scheme and explicit calculations of cloud water, ice, rainwater, and snow are simultaneously incorporated. Zhang et al. (1989) and Zhang and Gao (1989) showed that the model reproduced the meso-β-scale structure and evolution of the squall system extremely well, as verified against observational analyses by Augustine and Zipser (1987), Smull and Houze (1987), Johnson and Hamilton (1988), and Rutledge et al. (1988). Specifically, the model simulates well the initiation of the squall line at nearly the right time and location; the evolution of a mesovortex; the relative flow configuration of FTR motion at both upper and lower levels with an intermediate RTF flow; and the leading convective rainfall followed by a transition zone and stratiform precipitation. It should be pointed out, however, that the use of the 25-km grid length may have caused some aliasing of features on the subgrid scale, particularly those along

[1] All instabilities referred to in the text follow the definitions as given in the *Glossary of Meteorology* (Huschke 1959), except for symmetric instability, which is described in section 2.

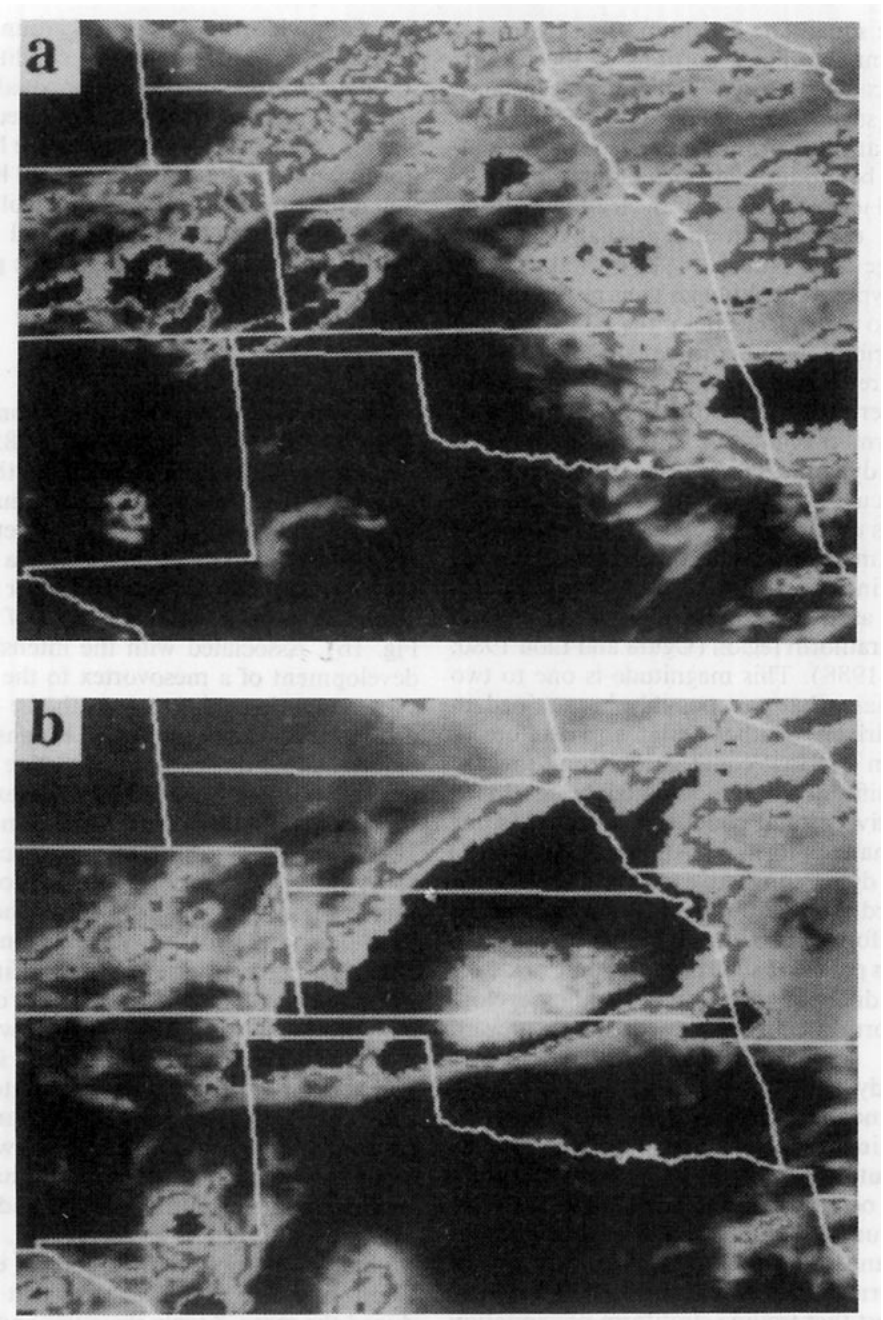

FIG. 1. Enhanced infrared satellite images for (a) 2100 UTC, (b) 0300 UTC, and (c) 0600 UTC; (d) composite low-level radar echo patterns for 0300 UTC (see Rutledge et al. 1988 for details) during 10–11 June 1985.

the leading line of the squall system. It is also likely that the lack of parameterization of cloud and precipitable substances in the Fritsch–Chappell scheme may to a certain degree affect the water budget of stratiform precipitation. Nevertheless, this simulation yields a dynamically consistent dataset with a resolution much higher than is possible from observations (e.g., the PRE-STORM network dataset). For a detailed description of the case and the model, the reader is referred to the aforementioned papers.

The MSI occurring in two dimensions has been extensively discussed in the literature (e.g., Hoskins 1974; Bennetts and Hoskins 1979; Emanuel 1979; Xu 1986) and widely accepted as a possible mechanism for the development of frontal rainbands (Parsons and Hobbs 1983; Knight and Hobbs 1987; Reuter and Yau 1990).

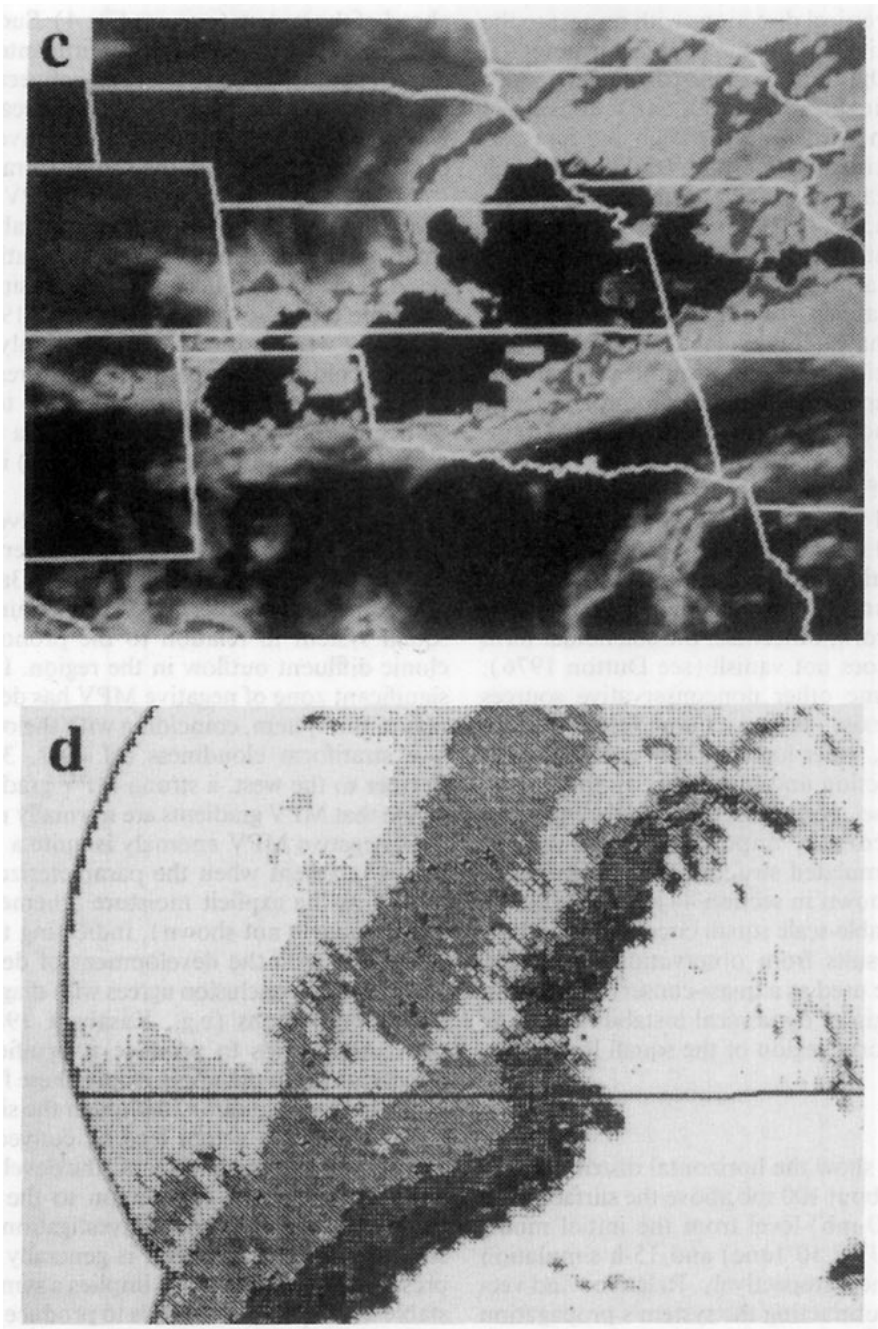

FIG. 1. (*Continued*)

According to Emanuel (1983a), MSI can be viewed as a result of unbalanced development of buoyancy forces in the vertical and centrifugal forces in the horizontal, thereby generating slantwise overturnings. In this sense, convective and inertial instabilities can be considered as special cases of MSI. The two-dimensional (2D) theory reveals that the atmosphere will be subject to MSI when it becomes saturated and has negative MPV. However, this instability will be conditional (CSI) when the atmosphere is unsaturated. In the 3D primitive equation model utilized here, MPV is given by

$$\text{MPV} = \frac{1}{\rho}\left[\frac{\partial\theta_e}{\partial n}\left(\frac{\partial w}{\partial s}-\frac{\partial v}{\partial z}\right)+\frac{\partial\theta_e}{\partial s}\left(\frac{\partial u}{\partial z}-\frac{\partial w}{\partial n}\right)+\frac{\partial\theta_e}{\partial z}\left(\frac{\partial v}{\partial n}-\frac{\partial u}{\partial s}+f\right)\right] \quad (1)$$

where u, v, and w are wind speeds (m s^{-1}) in the nor-

mal, parallel, and vertical directions with respect to the squall line, respectively; θ_e is the equivalent potential temperature; f is the local Coriolis parameter; and ρ is the density of air. From Eq. (1), MPV consists of contributions from baroclinity through the first two terms and convective and inertial stabilities through the last term. To take advantage of the linear nature of the squall system, Eq. (1) has been transformed from the model (x, y) into the right-hand (n, s) coordinates (with n axis normal to the line). For computational purposes, all derivatives in Eq. (1) were transformed from z to σ coordinates. It is evident from Eq. (1) that a negative correlation between absolute vertical vorticity and the θ_e lapse rate tends to produce negative MPV. As will be shown, this correlation tends to dominate the structure of 3D MPV in updraft regions of the squall system. If θ_e is replaced by θ, Eq. (1) becomes the Ertel's potential vorticity (see Dutton 1976, p. 383), which is conserved following an air parcel in an inviscid, continuous fluid. For a moist atmosphere, MPV is only conserved under saturated adiabatic conditions or in a 2D framework; otherwise, the solenoidal term (i.e., $\nabla\theta_e \times \nabla p$) does not vanish (see Dutton 1976). In this model, some other nonconservative sources (sinks) of MPV exist, such as numerical diffusion, freezing (melting), water loading, and, especially, parameterized convection and turbulence in the model. Nevertheless, these nonconservative processes are found to be of secondary importance in the present study, since the simulated structure and evolution of MPV (as will be shown in section 4) appear to be determined by resolvable-scale squall circulations and are consistent with results from observational analyses. Thus, MPV will be used as a quasi-conserved tracer to investigate the origin of dynamical instabilities taking place in the stratiform region of the squall line.

3. Evidence

Figures 2 and 3 show the horizontal distribution of MPV at a lower (about 100 mb above the surface) and an upper (i.e., 200-mb) level from the initial model condition (1200 UTC 10 June) and 15-h simulation (0300 UTC 11 June), respectively. Relative wind vectors, obtained by subtracting the system's propagation speed of 14.5 m s^{-1} normal to the leading line, as well as the position of the surface front and thermal boundaries relative to the ground, are also superposed. As shown by Zhang et al. (1989), the squall line was triggered mainly as a consequence of the interaction between the sector A cold front and the convectively unstable atmosphere associated with a quasi-stationary thermal boundary that extended from western Nebraska to eastern Oklahoma (Fig. 2b). Thus, a tongue of negative MPV resulting from convective instability was embedded in the southeasterly relative flow along the thermal boundary. Vertical cross-sectional analyses indicate the presence of negative MPV up to 600 mb ahead of the system (e.g., see Fig. 4). Such a thick layer of negative MPV is generally of little interest otherwise since it simply represents a deep convectively unstable environment. It is discussed here because this layer will be shown to be a source of negative MPV for the development of MSI in the squall's stratiform region.

At 200 mb (Fig. 2a), positive MPV is distributed everywhere except over northern Oklahoma, where a small and shallow area of slightly negative MPV is located. This area coincides with a dissipating MCS at this time (see Fig. 6a in Zhang et al. 1989). Note the relatively weak positive MPV anomaly ahead of the surface cold front that is believed to result from continued upward transport of the low- to midlevel air with small positive MPV induced by a midlevel short wave (see Fig. 3 in Zhang et al. 1989) in conjunction with the frontal circulation.

When the simulated squall line evolves into the mature stage, the MPV distribution differs dramatically from its initial pattern (cf. Figs. 2a and 3a). Specifically, a large area of smaller MPV has occurred above the squall system in relation to the pronounced anticyclonic diffluent outflow in the region. In particular, a significant zone of negative MPV has developed to the rear of the system, coinciding with the observed extensive stratiform cloudiness (cf. Figs. 3a and 1b–d). Farther to the west, a strong MPV gradient appeared. (Note that MPV gradients are normally not conserved.) This negative MPV anomaly is quite a significant signal. It is absent when the parameterized convection, as well as the explicit moisture scheme, is turned off in the model (not shown), indicating that it must be associated with the development of deep moist convection. This conclusion agrees with diagnostic analysis from observations (e.g., Kasahara 1982) that deep convection tends to produce a significant region of nonellipticity in the upper troposphere for the solution of the balance equation. Although the simulation may have aliased the actual leading convective line to a slightly wider convective zone, the development of this MPV anomaly and its relation to the squall system evidently warrant a careful investigation. In particular, since the stratiform region is generally saturated, the presence of negative MPV implies a symmetrically unstable atmosphere that tends to produce slantwise convection. Hence, the terms *stable* or *nonconvective* precipitation, traditionally used to refer to rainfall in this region, would seem to be inappropriate, based on the MPV concept.

In the low troposphere (Fig. 3b), the initial large area of organized negative MPV to the west of the PRE-STORM network is no longer present after the squall's passage. At this time, the squall system still continues to propagate into a convectively (of course, conditionally symmetric) unstable environment to the southeast but leaves behind a symmetrically stable air mass. Farther to the west, however, negative MPV appears again, although its magnitude is generally smaller than

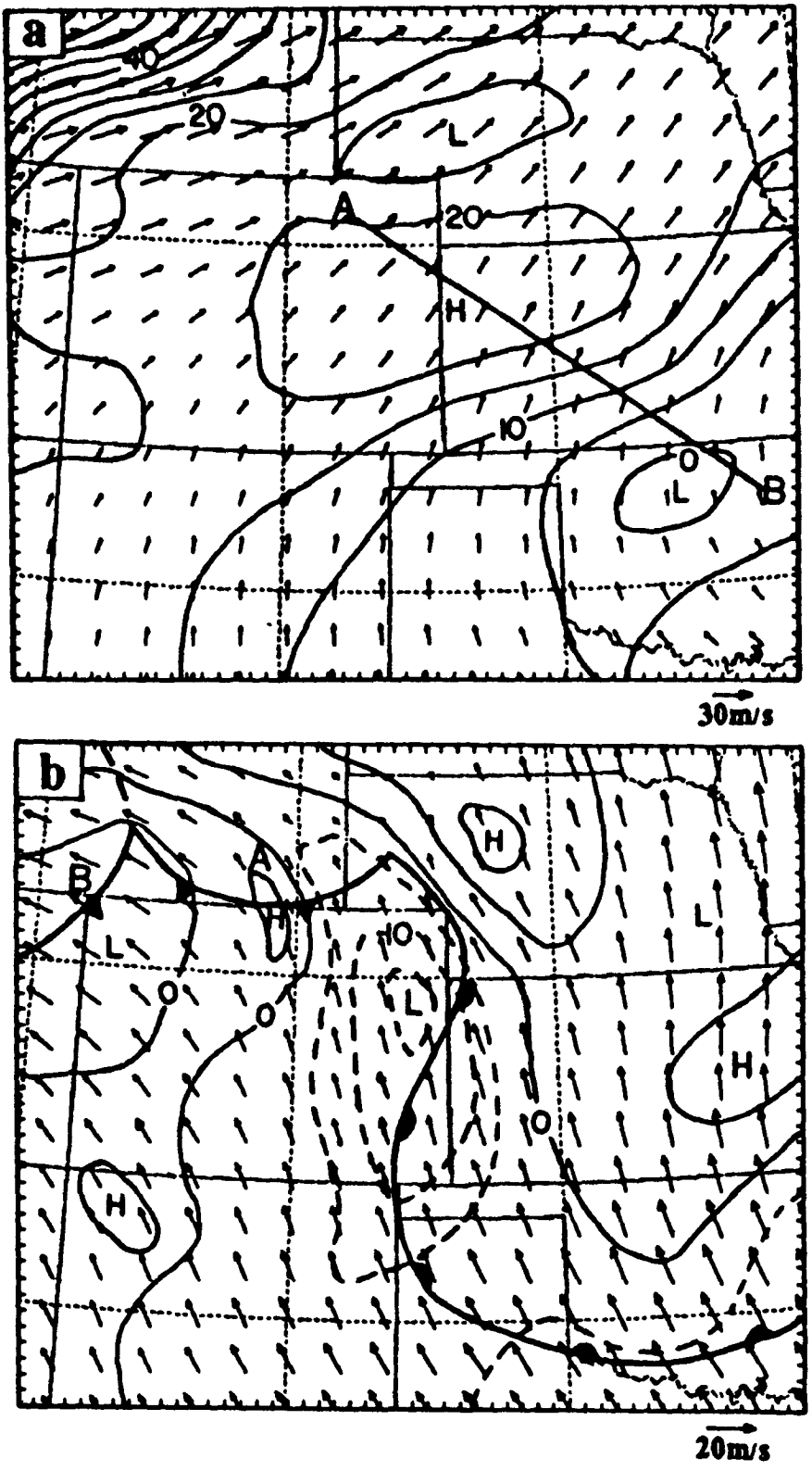

FIG. 2. Horizontal distribution of MPV at intervals of 5×10^{-6} m^2 K s^{-1} kg^{-1} superposed by relative wind vectors over a model subdomain at (a) 200 mb and (b) $\sigma = 0.873$ (about 100 mb above the surface) from the model initial time. Solid (dashed) lines indicate positive (negative) values. The thick solid line *AB* in (a) denotes the location of cross sections used for Figs. 4–14. The positions of the surface cold front and thermal boundaries are given in (b), and the letters A and B denote frontal sectors as discussed in the text. The intervals marked on the frame are fine grid-mesh grids (25 km); similarly in the rest of the figures.

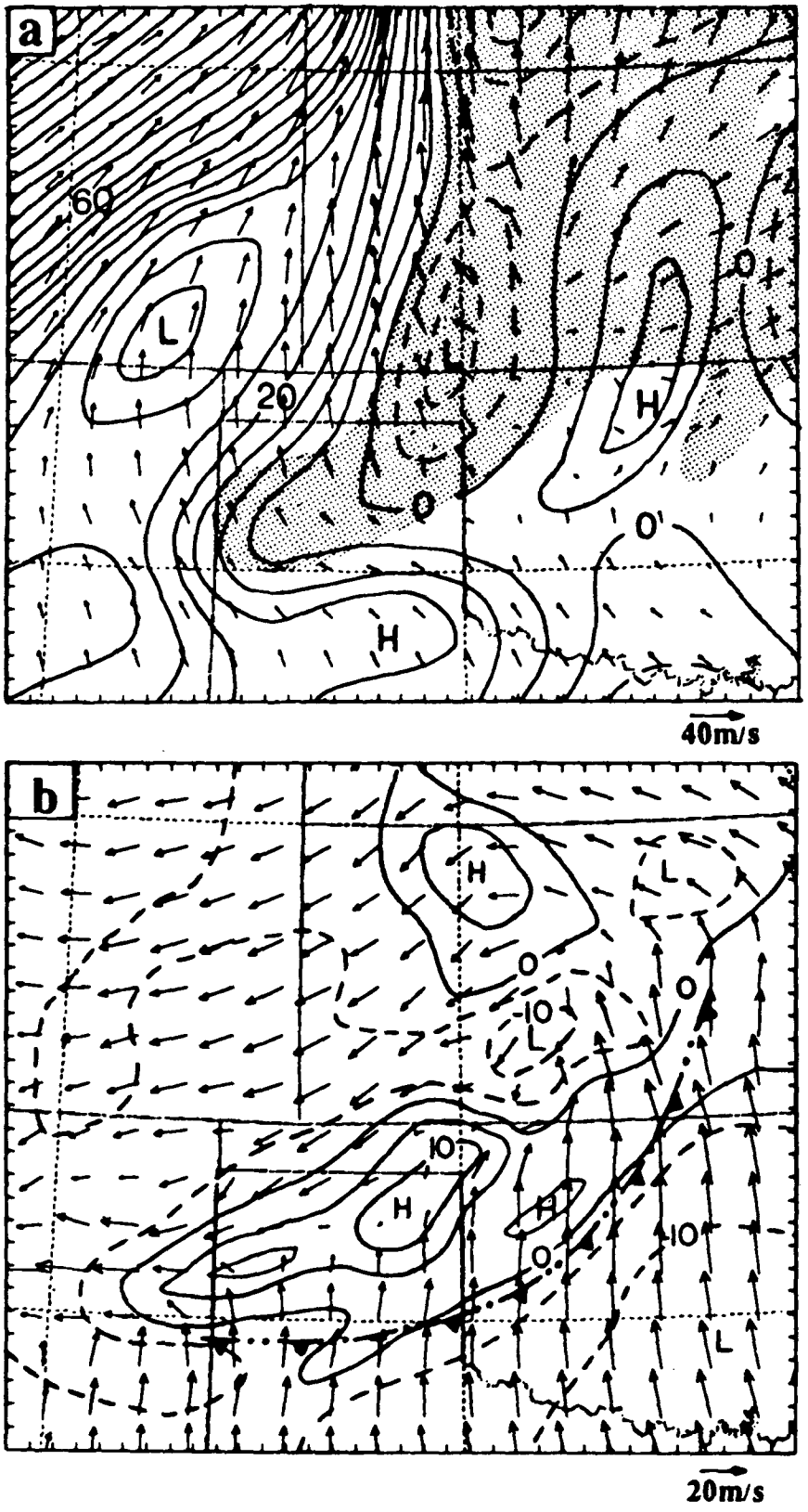

FIG. 3. As in Fig. 2 but from the 15-h simulation, valid at 0300 UTC 11 June 1985 and over a different model subdomain. Shadings in (a) denote relative humidity close to 100%. The leading cold outflow boundary in (b) is represented by cold-frontal symbols alternated with double dots.

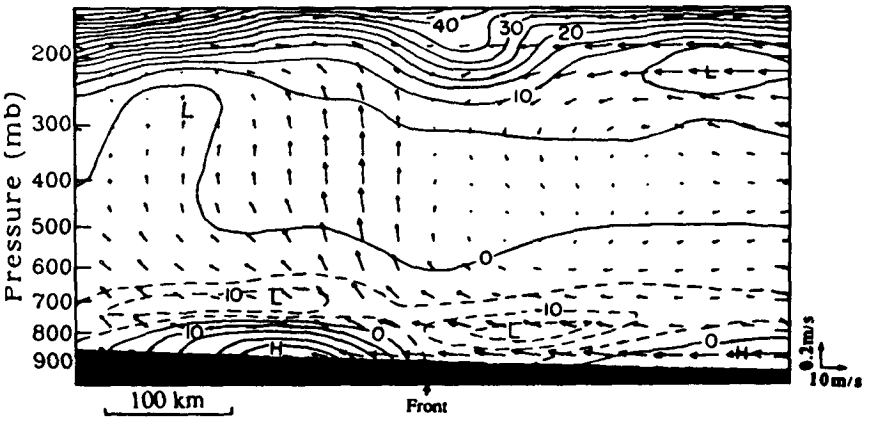

FIG. 4. Vertical cross section of MPV at intervals of 5×10^{-6} m^2 K s^{-1} kg^{-1} and relative circulation vectors along a segment of the line AB in Fig. 2a from 8-h simulation, valid at 2000 UTC 10 June 1985. Solid (dashed) lines indicate positive (negative) values. The cross section covers a horizontal size of 550 km.

that ahead of the system except over the area where stronger baroclinity associated with moist downdrafts occurred (see Zhang et al. 1989). This weak negative MPV appears to be associated with the observed development of scattered weak convective cells in the region (Rutledge et al. 1988; Johnson and Hamilton 1988). As will be shown in the next section, this negative MPV is transported from the boundary layer ahead of the system through the FTR flow and deposited here in a form of baroclinity with much less convective instability.

It should be mentioned that the presence of the positive MPV anomaly accompanied by a cyclonic wind circulation in the low troposphere and the negative MPV anomaly attended by anticyclonic flow at the upper levels resembles the hypothetical vertical PV structure of MCS's proposed by Raymond and Jiang (1990) but here shifted in phase in the vertical. With the above analyses and the quasi-conserved property of MPV in saturated air, it is hypothesized that the extensive area of negative MPV associated with stratiform rainfall results from upward transport of the boundary-layer unstable air mass through the squall-line circulation. This hypothesis is qualitatively[2] examined in the next section.

4. Structure and evolution

Figures 4–6 present vertical cross sections of MPV and relative circulation vectors along a line slightly to the south of the mesovortex center and nearly perpendicular to the squall line at the simulation times of 8, 12, and 15 h, which correspond to the presquall, developing, and mature stages, respectively. All cross sections lie within a fixed vertical plane but with different segments used to follow the system (see Fig. 2a). Prior to the squall's initiation (Fig. 4), the cold air behind the surface front is characterized by a positive MPV anomaly due to the presence of local large static stability and cyclonic vorticity. Ahead of and above the advancing surface front, the air is characterized by negative MPV that appears to be related to the development of the daytime convectively unstable boundary layer and the elevation of the boundary-layer air mass by frontal lifting. Together with the midlevel shortwave trough, the surface frontal system has organized a well-developed circulation prior to the squall's initiation; its maximum upward motion is about 20 cm s^{-1} (Fig. 4). Of particular interest is the development of a negative MPV bulge near 300 mb where upward motion lasts the longest. From modeling studies of Knight and Hobbs (1987) and Persson and Warner (1991), this bulge can be attributed to the upward lifting of lower-level negative MPV through the organized vertical motion above the surface front. Furthermore, the upper-level subsidence, driven by the larger-scale trough–ridge system and later also by convective mass compensation, tends to force packed MPV contours in the stratosphere downward and form a positive MPV anomaly immediately ahead of the squall system (see Figs. 3–6).

By $t = 12$ h (i.e., about 3 h after the initiation of the squall line), upward motion as strong as 1 m s^{-1} has developed, which has led to a deep saturated layer in the squall system (Fig. 5). Such strong upward motion appears to be closely related to resolvable-scale latent heat release. At this point, it may be helpful to reiterate individual roles of parameterized versus resolvable-scale convection in this particular simulation (see Zhang et al. 1988 for the more detailed discussion). Budget calculations, to be published elsewhere, indicate

[2] Quantitative examination of 3D MPV requires detailed budget and trajectory computations that could not be reliably performed with the available hourly model output in the present case.

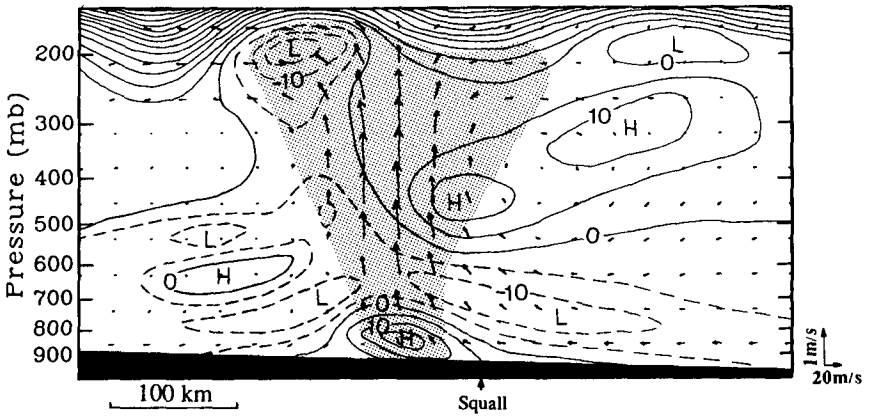

FIG. 5. As in Fig. 4 but from the 12-h simulation, valid at 0000 UTC 11 June 1985. Shadings indicate rainwater content larger than 0.2 g kg^{-1}.

that the magnitude of convective tendencies due to the Fritsch–Chappell (1980) scheme decreases rearward and vanishes in the stratiform region. The parameterized low-level cooling and drying contribute to the propagation of the squall system and the stabilization of its adjacent environment (see Zhang and Gao 1989), whereas the upper-level heating and detrainment moistening enhance lifting and produce moisture content sufficient for the later triggering of grid-box saturation in the stratiform region. Although convective updrafts produced by the Fritsch–Chappell scheme are as strong as 20–30 m s^{-1}, the resulting grid-scale upward motion along the leading line is much less than 1 m s^{-1}. This to some extent affects the upward transport of MPV and other cloud properties along the leading line in terms of timing and scale. In contrast, the occurrence of resolvable-scale condensation lags behind parameterized convection, and thus it contributes the most to stratiform precipitation. Meanwhile, because the grid-scale heating maximum is located at a lower level than the parameterized maximum, the resolvable-scale diabatic heating tends to determine the intensity of the FTR ascending flow as well as the structure and evolution of MPV. It should be pointed out that although the subgrid-scale momentum transport was excluded in this simulation because the model was found to be insensitive to the parameterized momentum flux in the scheme (Zhang and Fritsch 1988a), the model simulates well momentum transport processes associated with the squall system (Gao et al. 1990), as compared to observational budget computations by Gallus and Johnson (1992). Nevertheless, it still remains uncertain about the effects of subgrid-scale convection and turbulence on a specific realization of MPV (Shapiro 1976; Danielsen et al. 1987; Keyser and Rotunno 1990), since a clear understanding of these effects requires an explicit simulation of fully developed MCS's with much greater grid resolution.

Figure 5 also shows that the low-level negative MPV has been elevated above the surface cold pool and redistributed along the FTR ascending flow. It is partic-

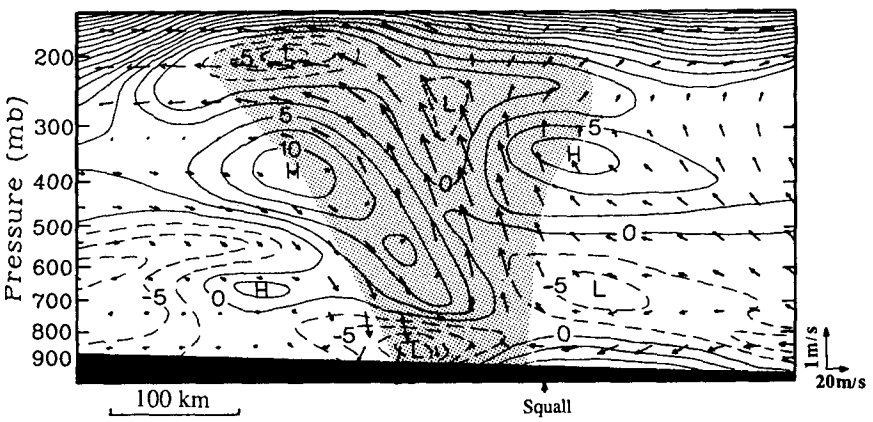

FIG. 6. As in Fig. 4 but at intervals of 2.5×10^{-6} m^2 K s^{-1} kg^{-1} from the 15-h simulation, valid at 0300 UTC 11 June 1985. Shadings indicate the region containing cloud substance.

ularly significant that large negative MPV, closely coupled with the low-level counterpart, has been deposited rapidly into the upper troposphere to the rear of the system, where the upward motion persisted the longest. This implies that the FTR ascending flow within the squall system is moist-symmetrically unstable, albeit to varying degrees. Note, however, that the maximum value of the negative MPV anomaly is somewhat larger than could possibly be found in the lower levels. This feature could be attributed to the use of the Fritsch–Chappell (1980) parameterization, in which MPV might not be conserved. Specifically, a portion of the negative MPV anomaly could be produced through the parameterized convective overshooting. Note also the relatively weak negative MPV in the middle portion of the FTR updrafts, which, to a certain degree, reflects the inhomogeneous distribution of MPV along the squall system (see the related discussion in Zhang and Gao 1989).

During the mature stage (Fig. 6) there are three distinct currents in the squall system: an overturning updraft ahead of the leading line, an FTR penetrative updraft, and an overturning downdraft, as defined by Thorpe et al. (1982) and detailed in Zhang and Gao (1989). At $t = 15$ h, a more extensive area of negative MPV occurs in the stratiform region, although its general magnitude has significantly decreased (cf. Figs. 5 and 6, and note different contour intervals used between these two figures) due to the rapid expansion of the stratiform region and also possibly to the effect of numerical diffusion. Despite the weakening, the upper-level MPV anomaly appears to be better coupled with the low-level counterpart through the FTR ascending flow than the one that occurred 3 h before. The boundary layer seems to be the source for the negative MPV in the upper troposphere, particularly when considering the FTR ascending motion being as strong as 1 m s^{-1}. Unlike the negative MPV in the system's wake, these coupled anomalies are embedded in the saturated ascending flow all the time. Thus, we may consider the development of stratiform precipitation partly as a result of the lifting of the lower-level moisture-rich air and the subsequent condensation (deposition) occurring within the slantwise airflow. This explanation does not contradict but rather complements the Smull–Houze (1985) hypothesis on the generation of stratiform rainfall. Specifically, some portion of precipitable water in the stratiform region could be advected rearward from the upper part of the leading convective line, but a significant portion may come from the boundary layer first through upright ascent and later through the FTR sloping flow. Furthermore, the leading convective cells would also leave behind a significant amount of water vapor for subsequent condensation (or deposition) in the FTR flow. This effect is partly treated in the model through moisture detrainment in the parameterized convection. Because these processes occur in a sloped ascending current, we may visualize the stratiform precipitation as an end product of slantwise convection.

To help illuminate how negative MPV appears at upper levels, MPV, as defined by Eq. (1), is decomposed into the baroclinic part and the convective-inertial part. A comparison between Figs. 6 and 7 indicates that the pattern and magnitude of 3D MPV in updraft regions are almost entirely determined by the product of convective stability and absolute vertical vorticity. Because of the presence of a θ_e minimum in a convectively unstable environment, the third term in Eq. (1) vanishes in the midtroposphere, as does the 3D MPV. Furthermore, the upwardly tilted zero isopleth terminates in the middle portion of the FTR updrafts where the sign of $\partial\theta_e/\partial z$ changes. These features may be the typical characteristics of MPV for MCS's that develop in a weak-gradient environment. Only in the lowest layers, the baroclinic terms have notable contributions to 3D MPV due to the presence of large wind shear ahead of the system. However, underneath the FTR ascending flows—that is, after the storm environment was significantly disturbed—both the first (i.e., the baroclinic effect normal to the line) and third components are of equal importance in determining the structure of 3D MPV. The second term in Eq. (1) involving baroclinity along the line appears to contribute the least to the 3D MPV (Fig. 7b), owing to small variability of θ_e along the line even though the vertical shear normal to the line is large. It should be pointed out that the baroclinic contributions are negligible prior to the initiation of the squall line except near the leading edge of the surface cold front.

A further decomposition of MPV portrays a region of negative vertical absolute vorticity in the top portion of the FTR ascending updrafts (Fig. 8), while the divergence field shows that the upper troposphere is highly divergent (Fig. 9). Furthermore, there is an indicatin of the development of a mesoscale jet stream to the northwest of the system (Fig. 3a). These characteristics, commonly associated with MCCs or mesovortices, have been observed by Ogura and Liou (1980), Fritsch and Maddox (1981), Fritsch and Brown (1982), Brandes (1990), and Menard and Fritsch (1989), and they have been simulated by Zhang and Fritsch (1988b). The results suggest that an air parcel following the FTR ascending current will be subject to convective instability ahead of the leading line and then to MSI in the stratiform region and to inertial instability in the upper portion of the system. Based on these results, it may be stated that the often-observed strong upper-level anticyclonic circulations associated with MCS's are a consequence of the upward transport of convectively unstable air in the boundary layer subject to the MPV conservation constraints.

Up to this point, we have not discussed why the wake region of the squall system still contains negative MPV (e.g., see Figs. 3b, 5, and 6), since it implies that not all the boundary-layer negative MPV could be

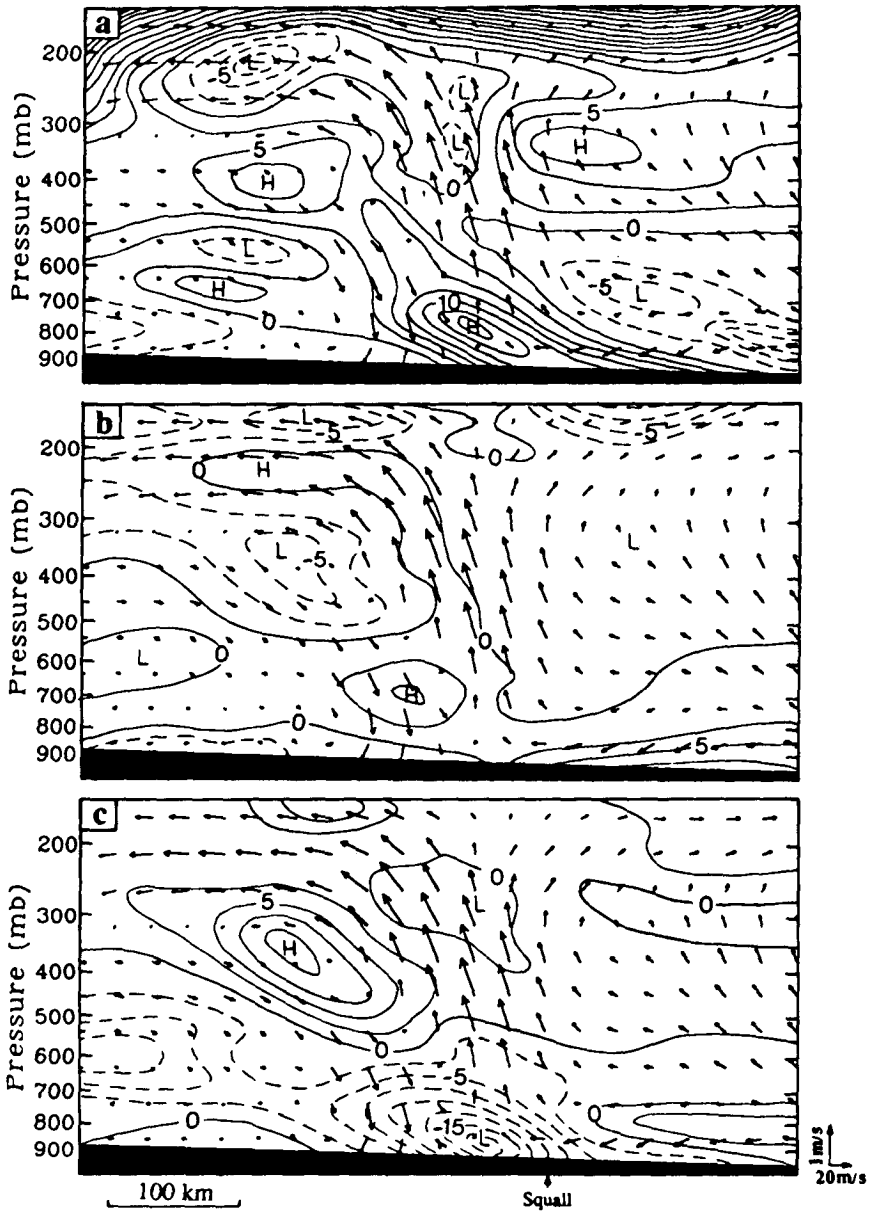

FIG. 7. As in Fig. 4 but at intervals of 2.5×10^{-6} m^2 K s^{-1} kg^{-1} for (a) the vertical component [i.e., $\partial\theta_e/\partial z\,(\partial v/\partial n - \partial u/\partial s + f)/\rho$]; (b) the along-line component [i.e., $\partial\theta_e/\partial s\,(\partial u/\partial z - \partial w/\partial n)/\rho$]; and (c) the across-line component [i.e., $\partial\theta_e/\partial n\,(\partial w/\partial s - (\partial v/\partial z)/\rho$] of MPV along a segment of the line *AB* in Fig. 2a from the 15-h simulation, valid at 0300 UTC 11 June 1985. Relative circulation vectors are superposed.

transported into the upper troposphere. It appears from the squall circulations presented in this paper and in Zhang and Gao (1989) that this negative MPV is transported by the FTR current, first ascending and later descending, from the boundary layer ahead of the system. As previously mentioned, the convective-inertial part dominates 3D MPV in the prestorm environment, yet it only contains a very small portion of negative MPV in the squall's wake region (Fig. 7a), indicating a significant decrease of convective instability after the squall's passage (also see θ_e distribution in Fig. 14). This process is well known as *convective adjustment* for the effects of upright convection on its environment (e.g., Newton 1950; Ogura and Liou 1980). With the MPV conservation constraints, it is found that most of the rearwardly transported negative MPV is stored in a form of baroclinity normal to the line in the system's wake (see Fig. 7c and θ_e distribution in Fig. 14). The generated baroclinity can also be seen from a vertical cross section of along-line flow in Fig.

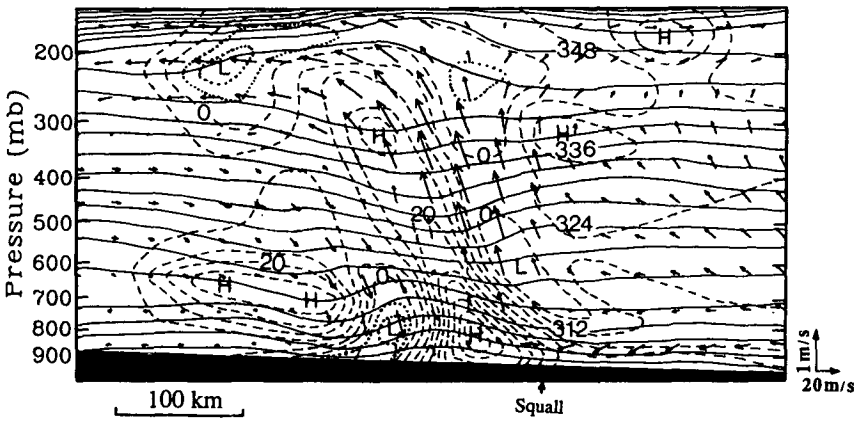

FIG. 8. Vertical cross section of virtual potential temperature (θ_v, solid lines) at intervals of 3 K and absolute vorticity (i.e., $\partial v/\partial n - \partial u/\partial s + f$) at intervals of 5×10^{-5} s^{-1}, superposed by relative-circulation vectors, along the line AB in Fig. 2a from the 15-h simulation, valid at 0300 UTC 11 June 1985. Dashed (dotted) lines denote positive (negative) absolute vorticity.

10, which shows slight vertical along-line shear ahead of the system but very strong shear behind the system. The question here is how to relate the convective instability ahead of the system to the large vertical along-line shear in the wake region. As we know, latent heating in a convectively unstable environment will give rise to upward motion. Zhang and Gao (1989) showed that as condensates in the ascending flow fall through a vertical unsaturated column, sublimative and evaporative melting cooling tends to force a descending rear-inflow jet. Then, as the RTF flow descends, the change in flow velocity should occur mostly in the direction parallel to the squall line, and this change is amount to the product of f (i.e., the Coriolis parameter) and the distance traveled by air parcels in the direction normal to the line, thereby producing large negative along-line winds at the lowest levels and strong vertical shear in the wake region. It is well known that the upper-level latent heating and lower-level evaporative cooling tends to vertically stabilize the thermodynamic conditions, based on the theory of conditional instability. According to the MSI theory, however, the corresponding flow fields have to be modified in such a way as to satisfy the MPV conservation constraints. Hence, the presence of strong wind shear in the squall's wake is a consequence of slantwise adjustments between mass and wind fields following the occurrence of latent heating and cooling. It should be mentioned that horizontal advection of MPV from the squall's adjacent environment could also be significant in determining the magnitude of negative MPV in the wake region.

Note that although the baroclinic generation outweighs the convective-inertial contribution in determining the sign of 3D MPV near the leading edge of moist downdrafts in this particular cross section (e.g.,

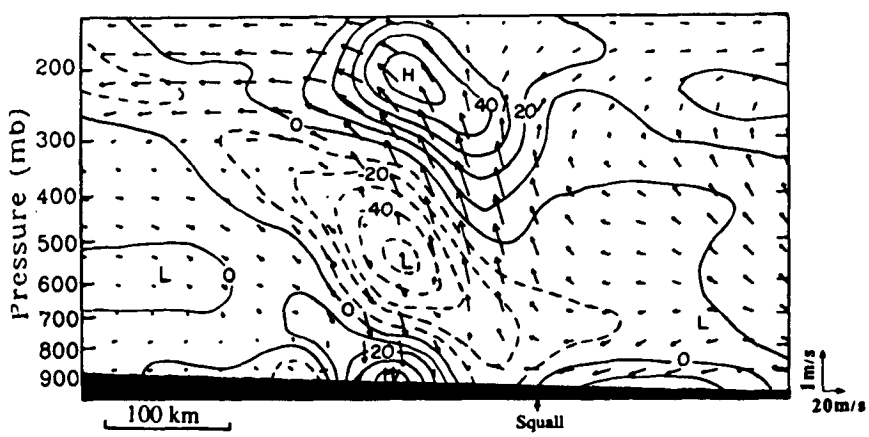

FIG. 9. Vertical cross section of divergence (i.e., $\partial u/\partial n + \partial v/\partial s$) at intervals of 10^{-4} s^{-1}, superposed by relative circulation vectors along a segment of the line AB in Fig. 2a from 15-h simulation, valid at 0300 UTC 11 June 1985. Solid (dashed) lines denotes divergence (convergence).

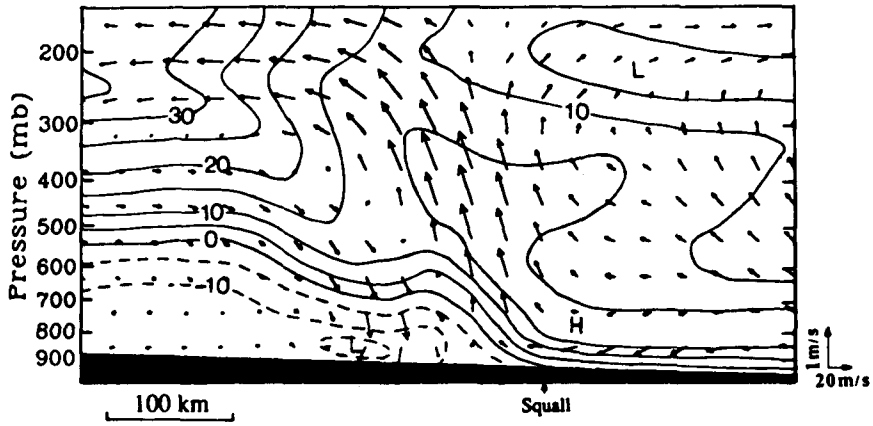

FIG. 10. As in Fig. 9 but for the horizontal winds along the squall line at intervals of 5 m s^{-1}. Solid (dashed) lines indicate flow into (out of) the page.

Figs. 6–7), positive MPV generally occurs in the lowest layers immediately behind the leading line (see Fig. 3b). This is because sublimative–evaporative cooling and parameterized downdrafts tend to force the midlevel lower-θ_e air to descend so that convective stability, mass convergence, and cyclonic vorticity increase near the squall front. However, this large positive MPV does not appear to be entirely transported from the middle to upper tropospheres or from preexisting positive MPV associated with the surface front. Some local nonconservative processes, such as the solenoidal term near the squall front, melting and freezing, boundary-layer mixing, and a portion of the parameterized downdraft effects, seem to have partly contributed to its formation. Nonetheless, toward the back edge of the system, this positive MPV diminishes due to the continued downward and forward erosion of negative MPV (in a form of baroclinity) from higher levels (see Figs. 6, 7, and also 15a), which is consistent with an increase of the along-line vertical shear toward the leading edge of the descending rear inflow (Fig. 10). Note also that the flow along the interface is symmetrically stable primarily due to the presence of large negative vertical shear along the line in correlation with a rearward decrease of θ_e (cf. Figs. 6, 7c, 10, and θ_e distribution in Fig. 14), but it is dynamically unstable (i.e., with a Richardson number as small as 0.4 in a model layer of 50 mb) due to large vertical shear (Fig. 7b).

It is worth noting the two vorticity maxima within the squall system: one is located at 800 mb near the leading line, and another is the mesovortex sometimes referred to in the stratiform region of MCS's (Fig. 8). The two vorticity maxima appear to develop with different mechanisms. Specifically, the former seems to result mainly from the low-level convergence in response to latent heating in the FTR updrafts, whereas the latter is produced by weak vortex stretching (due to midlevel convergence) that is followed by strong tilting of horizontal vorticity normal to the line (due to the presence of strong vertical shear). It is of particular interest that the mesovortex in the stratiform region develops in the RTF descending current, as opposed to that in the mesoscale ascent, such as the one near the leading line in the present case, and many other MCC-related mesovortices (e.g., Leary and Rappaport 1987; Zhang and Fritsch 1987, 1988b; Kuo et al. 1988; Menard and Fritsch 1989). Johnson et al. (1990) have recently reported a similar mesovortex that developed in the descending flow of an MCS during PRE-STORM. It is interesting to note that the mesovortex associated with the FTR ascending flow exhibits a warm-core structure, whereas the one in the descending flow is characterized by upper-level cooling and low-level warming. A detailed analysis of the vorticies will be published in a forthcoming journal article.

Since this study attempts to treat the flow regime in a stratiform region as slantwise convection, Figs. 11 and 12 display vertical cross-sectional analyses of buoyancy ($g\,\Delta\theta_v/\bar{\theta}_v$, where $\Delta\theta_v$ is a perturbation over the four-point average $\bar{\theta}_v$) and centrifugal forces (fv_{ag}, where v_{ag} is the ageostrophic wind component along the squall system), both having a unit of 10^{-3} m s^{-2}. On average, the buoyancy forces are about one order of magnitude smaller than typically appear in deep convective storms but one order of magnitude greater than could possibly be attained in frontal rainbands. It is apparent that the stratiform region is dominated by sloping positive buoyancy and negative centrifugal forces. Thus, the resultant of these two forces will enhance the FTR slantwise convective motion within the stratiform region, and MSI could indeed be viewed as buoyant inertial instability (Emanuel 1983b). Note though that the positive buoyancy is maximized in the midtroposphere, which coincides with the strongest resolvable-scale heating, whereas the largest ageostrophic acceleration occurs in the upper troposphere, where the strong anticyclonic and divergent flow prevails.

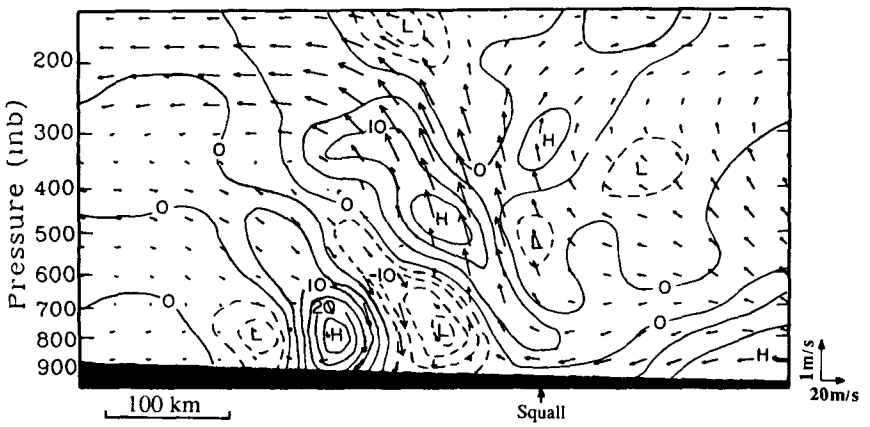

FIG. 11. As in Fig. 9 but for buoyancy forces ($g\,\Delta\theta_v/\overline{\theta_v}$) at intervals of 5×10^{-3} m s^{-2}. Solid (dashed) lines denote upward (downward) buoyancy acceleration.

Numerical momentum budgets for this case also show that the upward and rearward acceleration is a result of an imbalance among the pressure gradient force, the Coriolis force, and the vertical advection of horizontal momentum (see Fig. 9 in Gao et al. 1990).

If we regard the development of the aforementioned upward and rearward acceleration entirely as a consequence of local imbalances associated with diabatic heating, let us look at background flow conditions prior to the initiation of the squall line, based on the Lagrangian parcel theory of MSI by Emanuel (1983b). Figure 13 shows the vertical cross section of absolute momentum ($M = v + fn$) and θ_e normal to the line at $t = 8$ h. Because the along-line flow increases with height, M increases upward and with distance normal to the line. Above 300 mb, M begins to tilt rearward behind the surface front. Meanwhile, the basic state in the lower troposphere displays pronounced convective instability, particularly near the frontal zone (cf. Figs. 4 and 13). Thus, if we follow an air parcel taken from the unstable boundary layer in a Lagrangian sense, the upward and rearward acceleration can be definitely expected in this 2D framework, assuming that the background flow is subgeostrophic in the boundary layer and geostrophic above. Furthermore, the environmental meso-α-scale pressure distribution also tends to produce rearward acceleration of the background flow, since the squall system propagates from the short-wave trough to the ridge region to the east (see Fig. 3 in Zhang et al. 1989 and Zhang and Gao 1989). In fact, even at this time, the basic state already exhibits an upward and rearward component of the flow near the leading frontal zone (see Fig. 4). On the other hand, if M can be considered as a conserved variable, which is true for a purely 2D case, the vertical release of convective instability also requires upward and rearward movements of air parcels. All of the aforementioned results further support the previous discussion that convective instability with upright convection occurs ahead of the leading line, MSI with slantwise convec-

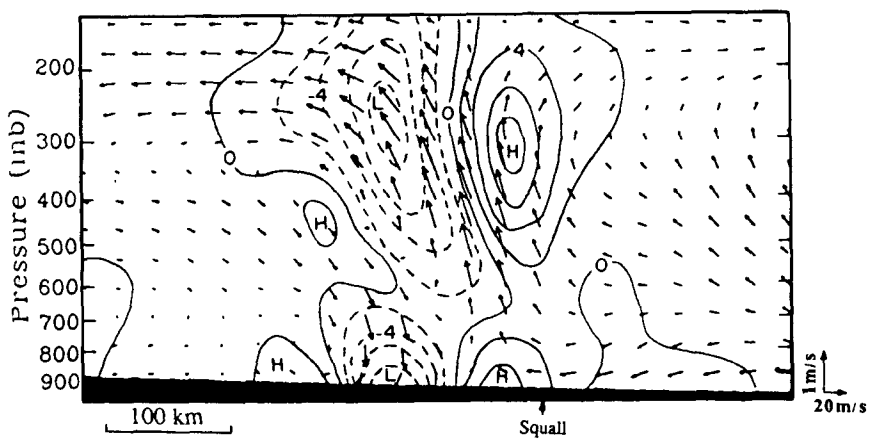

FIG. 12. As in Fig. 9 but for centrifugal forces (fv_{ag}) at intervals of 2×10^{-3} m s^{-2} where v_{ag} denotes ageostrophic winds along the squall line. Solid (dashed) lines indicate leftward (rightward) acceleration of the flow normal to the squall line.

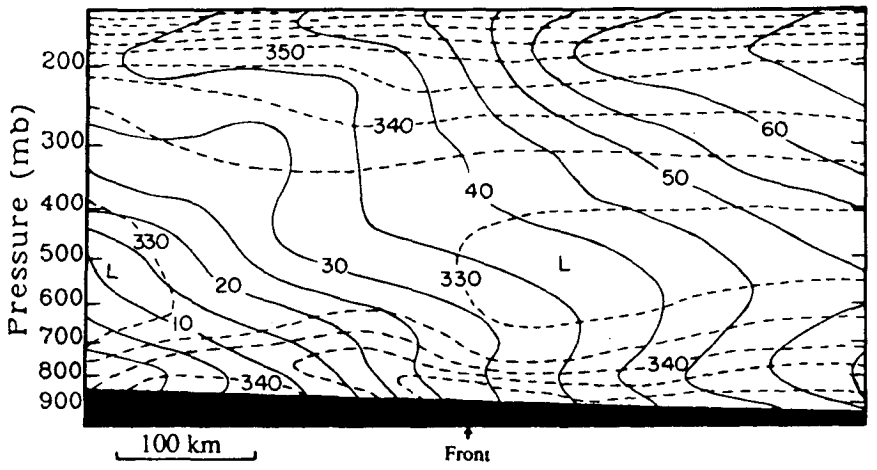

FIG. 13. Vertical cross section of absolute momentum (solid lines) at intervals of 5 m s^{-1} and θ_e (dashed lines) at intervals of 5 K along a segment of the line AB in Fig. 2a from the 8-h simulation, valid at 2000 UTC 10 June 1985.

tion occurs in the stratiform region, and inertial instability with strong radial unbalanced flow occurs near the tropopause.

After convection has taken place for several hours, the vertical M and θ_e distributions in the storm environment have been significantly altered. First, slantwise convection has produced a deep layer of constant θ_e surfaces tilted from the leading line to the back edge of the stratiform region and has, consequently, left behind significant baroclinity in the low to midlevels (Fig. 14). These features bear remarkable resemblance to those observed by Newton (1950), Ogura and Liou (1980), Zipser et al. (1981), and others. Although pronounced convective instability is still present ahead of the system (now above the nocturnal boundary layer), it has been gradually removed toward the rear. It is important to note that the vertical θ_e gradient near the tropopause, though still positive, has decreased markedly due to continued convective heating and moistening. This indicates the tendency of upper-tropospheric convective destabilization by the squall system. In nature, there might still be shallow, small-scale upright convection going on in the stratiform region. In fact, slantwise convection has generated a slightly negative θ_e lapse rate in the core of the FTR ascending flow as a result of upward transport of high-θ_e air. Second, the aforementioned three air currents have modified the structure of constant M surfaces as if they were conserved (see Gao et al. 1990). Thus, M surfaces roughly follow the streamlines of overturning updrafts ahead of the system and tilt rearward and even become horizontally oriented in the stratiform region. As a result, the stratiform region is dominated by a negative horizontal gradient of M (i.e., $\partial M/\partial n$), which is consistent with the distribution of negative absolute vorticity in the region (cf. Figs. 8 and 14).

With the aid of Fig. 14, we can understand better why the inertial-convective contribution dominates 3D

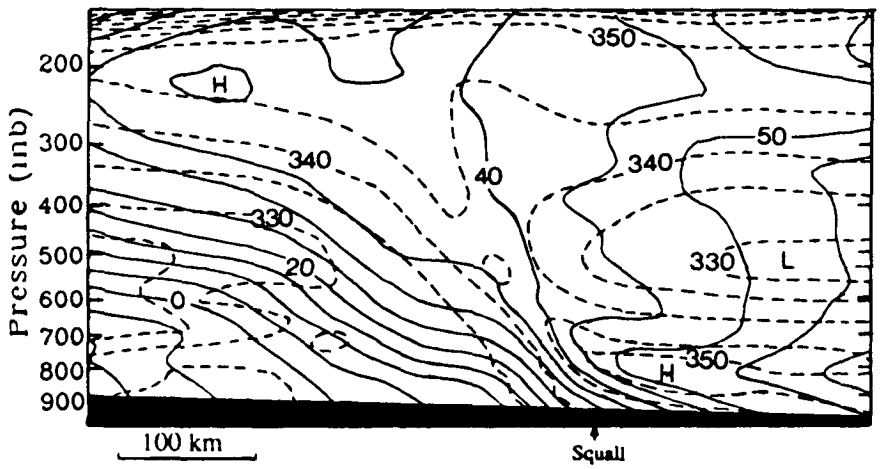

FIG. 14. As in Fig. 13 but from the 15-h simulation, valid at 0300 UTC 11 June 1985.

MPV in the updraft regions. As shown in Figs. 8 and 14, the ascending motion occurs in association with penetrative constant-θ_e surfaces (θ_e = 340 K in this case). Thus, horizontal θ_e gradients within the updraft core nearly vanish across the θ_e surfaces. As an air parcel reaches the upper troposphere, its θ_e value will be smaller than that from above. This implies that absolute vorticity has to be negative, which leads to the development of the often-observed strong anticyclonic outflows near the top of MCS's. It is evident that larger negative MPV in the convective roots would more likely result in stronger anticyclonic divergent outflow near the tropopause.

If we can piece all of the aforementioned information together, the following concepts can be obtained for this particular case. Near the leading line, convective instability determines 3D negative MPV, and thus, upright convection is responsible for vertically stabilizing the atmospheric column. Because the along-line flow increases with height in the lower troposphere, some ascending parcels from the boundary layer will be subject to rearward acceleration and, thus, enter the stratiform region. Although purely upward displacement is stable behind the leading line, saturated air parcels, if lifted along slantwise M surfaces (say between 35 and 40 m s^{-1}), will experience substantially smaller environmental θ_e and will accelerate upward and rearward along the slantwise surfaces. As the parcels ascend, some portion of negative MPV is transported upward and rearward and eventually deposited into the upper troposphere, while the remaining portion is transported rearward in the lower troposphere through the FTR flow and later deposited mostly in a form of baroclinity in the system's wake. Because of the Coriolis effect, air parcels in both the FTR and RTF flows will be displaced anticyclonically [see Figs. 3a,b and also air trajectories in Fig. 11a of Zhang and Gao (1989)], thus having the tendency to produce negative absolute vorticity in the lowest and upmost layers. The penetrative constant-θ_e surfaces and a decrease in convective stability within the stratiform region facilitate the undilute slantwise ascent of the boundary-layer air into the upper levels for the generation of strong upward motion and stratiform precipitation. As the air approaches the back edge of the system, less moisture is available for latent heat release (see Fig. 10); therefore, the ascending component of the FTR flow weakens and becomes inertially unstable when negative absolute vorticity dominates 3D MPV. In the lower portion of the FTR ascending flow, evaporative (melting) cooling tends to induce the descent of midlevel lower-θ_e air into the lowest layers so as to vertically stabilize the lower troposphere. In the meantime, the resulting descending rear-inflow enhances mass convergence and cyclonic vorticity near its leading edge. Thus, a positive contribution to 3D MPV occurs, implying a symmetric stabilization of the boundary layer. Therefore, deep moist convection tends to remove lower-level convective instability ahead of the system and transform this instability into MSI during the slantwise upward transport in such a way as to symmetrically destabilize the middle-to-upper troposphere. This slantwise adjustment may be understood as the upward transport of negative MPV along slantwise constant θ_e surfaces by reversing the signs of both $\partial\theta_e/\partial z$ and absolute vorticity (i.e., $\partial v/\partial n - \partial u/\partial s + f$). This process differs from purely vertical adjustment, in which only thermodynamic alteration is required. The results clearly reveal that the significant negative MPV in the stratiform region of this simulated squall system is not entirely due to certain nonconservative processes inherent in the present model, since the previously mentioned θ_e and absolute vorticity structures have more or less been observed (e.g., Newton 1950; Ogura and Liou 1980; Menard and Fritsch 1989).

The aforementioned MPV transport concept has interesting implications for parameterization of moist convection. In particular, all of the cumulus parameterization schemes developed so far have excluded subgrid-scale transport of horizontal momenta. As we know, those schemes normally produce a heating and moistening maximum at an upper level, though in general agreement with observational budget computations for midlatitude MCS's (e.g., McNab and Betts 1978; Kuo and Anthes 1984; Gallus and Johnson 1991). It is evident that this heating–moistening profile tends to thermodynamically stabilize the lower troposphere and rapidly induce low-level convergence and upper-level divergence. However, the rotational component of the wind fields due to convective developments, which is important for realistically predicting meso- and larger-scale weather systems, has to be geostrophically adjusted with a time lag. This adjustment process is very slow over tropic regions. Therefore, it appears to be logically appropriate, as a first approximation, to include convective momentum transport into cumulus parameterization schemes based on the correlation between convective stability and vertical absolute vorticity.

To gain insight into the influence of the squall system on the larger-scale environment, Fig. 15a presents the vertical distribution of MPV and circulation vectors at a much larger scale from the 18-h simulation, valid at 0600 UTC 11 June. Note that the system at this time was rapidly dissipating (Fig. 1c) as it propagated into a convectively less unstable (or less negative MPV) environment. Hence, the previously mentioned coupling of MPV between the lower and upper levels is no longer present during this decaying stage. However, the low-level cooling (drying) and the upper-level heating (moistening) of the squall system, as shown in Fig. 20 of Zhang and Gao (1989), have resulted in negative MPV anomalies near the tropopause and a positive MPV anomaly in the boundary layer, except several hundreds of kilometers behind the leading line. As already mentioned, the descending rear inflow, in-

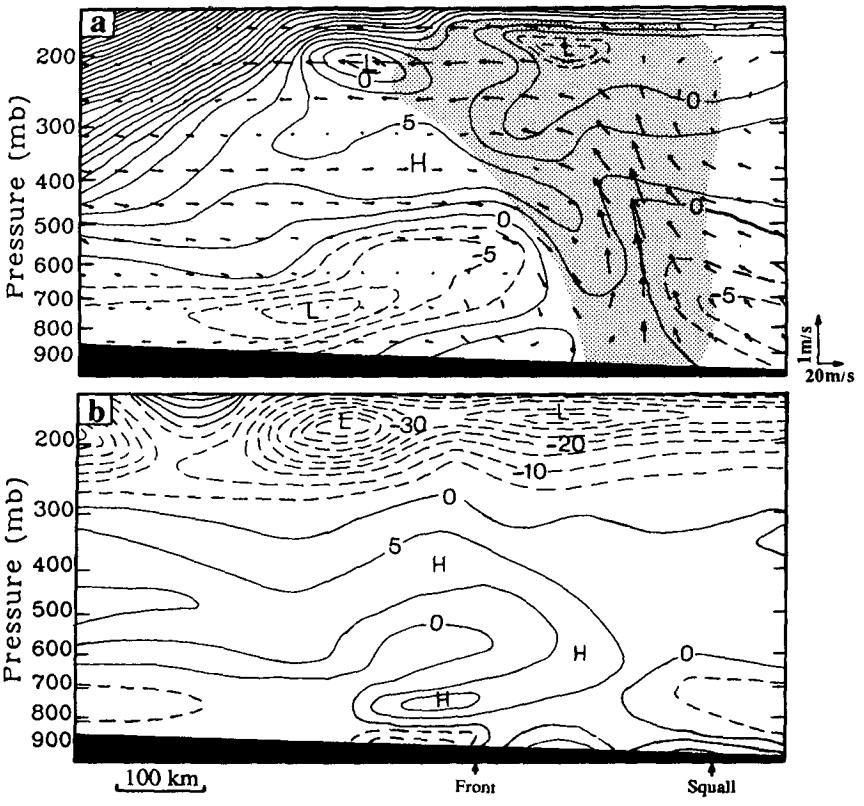

FIG. 15. (a) As in Fig. 4 but at intervals of 2.5×10^{-6} m^2 K s^{-1} kg^{-1} from the 18-h simulation, valid at 0600 UTC 11 June 1985 (shadings denote rainwater content larger than 0.2 g kg^{-1}); and (b) the vertical cross section of the deviation MPV at intervals of 5×10^{-6} m^2 K s^{-1} kg^{-1} between the control and no diabatic heating runs from the 18-h simulation. The cross section is taken along the same line as for all previous figures but covers a horizontal size of 850 km.

duced by sublimative and evaporative cooling, tends to transport midlevel negative MPV forward to diminish the cooling-related positive MPV anomaly at lower levels. Meanwhile, the packed upper-level MPV contours have been significantly elevated by the squall system. Near the back edge of the squall circulation the large positive MPV appears to be associated with stratospheric air that has descended into the midtroposphere.

Finally, to see how significant the net effect of slantwise convection is on the larger-scale environment, an additional numerical experiment was run in which neither convective nor resolvable-scale condensational heating (NDH) was included (see Zhang and Fritsch 1988a for further description). The simulation presumably produces the evolution of the larger-scale basic state without the influence of the squall system. Thus, by subtracting the basic state from the control run, the perturbations generated by the squall system can be isolated. As shown in Fig. 15b, the largest symmetrically generated perturbations also occur in the lowest and the uppermost layers. The squall system tends to draw negative MPV air from the boundary layer, transport it into the upper troposphere (i.e., above 300 mb), and leave behind less negative MPV air in the lower half of the troposphere. Because the shallow surface cold front in experiment NDH propagates much slower than the control-simulated squall front (see Fig. 18 in Zhang and Gao 1989), the large positive MPV associated with the cold front yields negative MPV deviations when subtracted from that in the control simulation. The upper portion of the stratiform region is filled with a deep layer of large negative MPV deviations. It is also apparent that the net effect of the squall system is to stabilize the lower troposphere and destabilize the upper troposphere with respect to MSI.

5. Discussion and conclusions

In this study, evidence has been presented on the development of an extensive area of negative moist potential vorticity (MPV) or moist symmetric instability (MSI) in the stratiform region of a midlatitude squall line, based on a 3D high-resolution numerical simulation of a case that occurred on 10–11 June 1985 during PRE-STORM. It has been shown that the broad stratiform region is quite stable to pure upward displacement but considerably unstable to slantwise convection. The presence of this pronounced slantwise

convective instability can help explain the generation of a large amount of stratiform precipitation in the present squall system. The evolution of MPV has been diagnosed to trace the origin of dynamical instabilities taking place in the squall system. The results appear to reveal that this large area of negative MPV is generated as a result of upward transport of boundary-layer convectively unstable air in the front-to-rear (FTR) sloping flow by reversing the sign of $\partial\theta_e/\partial z$ and absolute vertical vorticity. Thus, this upward transport could lead to the often-observed development of strong anticyclonic and divergent outflow in the upper troposphere. In a certain sense, the presence of MSI in the squall stratiform region can be regarded as a residue of convective instability along the sloping surface after vertical stabilization by upright convection. Then, a residue of MSI after slantwise adjustment will be transformed into pure inertial instability in the upper troposphere. The effect of slantwise convection is to symmetrically stabilize the lower troposphere and inertially destabilize the upper troposphere. It is also found that some portion of negative MPV ahead of the squall system is transported rearward through the FTR current, first ascending and then descending, and later deposited in a form of baroclinity with much less convective instability in the system's wake. The results indicate that an air parcel following the FTR ascending flow will evolve from pure updrafts with convective instability over the leading portion of the system, slantwise ascent with MSI within the stratiform region, and pure horizontal outward acceleration with inertial instability in the upper troposphere. The results also suggest that the effects of convective momentum transport could be incorporated into meso- or larger-scale models based on the correlation between absolute vorticity and convective stability.

Although these conclusions are only drawn from a single simulation study, they are well supported by recent observations of mesoscale convective systems. In particular, Leary and Rappaport (1987) observed strong anticyclonic flow in the upper troposphere and the banded structure of precipitation pattern with weak reflectivity in the stratiform region of a mature mesoscale convective complex. They also documented convectively near-neutral lapse rate and continued overturning within the rainbands in conjunction with an FTR ascending flow. Their observations appear to support our conjecture about the transformation processes from convective instability ahead of the system to MSI in the stratiform region, with the latter being responsible for the development and maintenance of the rainbands. In addition, Fritsch and Brown (1982), Brandes (1990), and Menard and Fritsch (1989) reported the development of highly divergent outflow with negative absolute vorticity in the upper troposphere associated with MCCs, in agreement with our hypothesis.

The present findings appear to have significant implications with respect to the development of rapid, intense oceanic storms. In particular, recent field experiments such as GALE (Genesis of Atlantic Lows Experiment, Dirks et al. 1988) and ERICA (Experiment on Rapidly Intensifying Cyclones over the Atlantic, Hadlock and Kreitzberg 1988) have measured 10°–20°C temperature difference between the sea surface and cold air flowing over the Gulf Stream ahead of cyclones. This is clearly a convectively unstable condition, at least in the lowest boundary layer, and has been observed to be responsible for frequent convective outbreaks along the leading surface fronts. It is quite possible that this convectively unstable air would be transported into the frontal zone to aid in the development of MSI, then released in the form of the slantwise convection during the rapid deepening processes, and eventually left with strong anticyclonic flow in the upper troposphere, a scenario similar to the case presented herein. This concept seems to be reasonably supported by a numerical simulation of the ERICA IOP 4 storm by Shapiro et al. (1991). On the other hand, the 2D flow structure in the present squall system is analogous to an advancing katabatic cold front overrun by FTR ascending warmer air but on a different scale. If this can be the case, the stratiform region, as displayed in Fig. 1d, may be viewed as if it were a rainband in the frontal system. Then, some of the present findings could be applied to those cases of explosive cyclogeneses. Thus, it appears that more studies focusing on the relationships between air–sea interactions and MSI associated with oceanic cyclogeneses are necessary to help understand the physical mechanisms controlling the formation and rapid development of those storms.

It is important to point out, however, that the results and implications presented herein are obtained only from a single numerical case study in which numerous approximations are made. It is also important to point out that the present study represents the first effort to relate the squall stratiform precipitation to MSI. Several outstanding questions still remain to be answered. For instance, to what extent is MSI responsible for the development of the FTR flow and stratiform precipitation? How does the energy transfer between the background flow and squall circulation take place in the MSI region? What is the final destiny of the negative MPV near the tropopause? Thus, further quantitative investigations are needed to help clarify the relationships among stratiform precipitation, leading upright convection, and their environmental conditions and to determine the roles of convective, symmetric, and inertial instabilities and their interactions in the formation and evolution of squall lines as an integral system. In particular, it is necessary to conduct fully explicit simulations of MCS's, namely with 3D cloud models, and to trace the evolution of MPV from the boundary layer to the stratiform region. Furthermore, attempts should be made in future field experiments

to measure both upright and slantwise instabilities inside and outside of MCS's, such as thermodynamic soundings along absolute momentum surfaces, as demonstrated by Emanuel (1988). If the findings presented in this study can be confirmed, the present views on the treatment of moist convection in numerical models, as well as numerical simulations of MCS's, may need to be revised.

Acknowledgments. We wish to thank Mr. Kun Gao for his assistance in preparing the hourly model output for the present study, and Drs. K. Emanuel, M. Shapiro, and T. Warn for their helpful discussions. We are grateful to Drs. M. K. Yau, D. Keyser, and two anonymous reviewers for their constructive comments. The drafting expertise of Ms. Ursula Seidenfuss in figure preparation is acknowledged. The model integration was performed on CRAY X-MP of the National Center for Atmospheric Research, which is sponsored by the National Science Foundation. The research was partly supported by the Natural Science and Engineering Research Council and Atmospheric Environmental Service of Canada.

REFERENCES

Anthes, R. A., E.-Y. Hsie, and Y.-H. Kuo, 1987: Description of the Penn State/NCAR mesoscale model version 4 (MM4). Tech. Note, NCAR/TN-282, 66 pp.

Augustine, J. A., and E. J. Zipser, 1987: The use of wind profilers in a mesoscale experiment. *Bull. Amer. Meteor. Soc.*, **68**, 4–17.

Bennetts, D. A., and B. J. Hoskins, 1979: Conditional symmetric instability—A possible explanation for frontal rainbands. *Quart. J. Roy. Meteor. Soc.*, **105**, 945–962.

Brandes, E. A., 1990: Evolution and structure of the 6–7 May 1985 mesoscale convective system and associated vortex. *Mon. Wea. Rev.*, **118**, 109–127.

Churchill, D. D., and R. A. Houze, Jr., 1984: Development and structure of winter monsoon cloud clusters on 10 December 1978. *J. Atmos. Sci.*, **41**, 933–960.

Cunning, J. B., 1986: The Oklahoma–Kansas Preliminary Regional Experiment for STORM-Central. *Bull. Amer. Meteor. Soc.*, **67**, 1478–1486.

Danielsen, E. F., S. E. Gaines, G. W. Sachse, G. L. Gregory, and G. F. Hill, 1987: Three-dimensional analysis of potential vorticity associated with tropopause folds and observed variations of ozone and carbon monoxide. *J. Geophy. Res.*, **92**, 2103–2111.

Dirks, R. A., J. P. Kuettner, and J. A. Moore, 1988: Genesis of Atlantic Lows Experiment (GALE): An overview. *Bull. Amer. Meteor. Soc.*, **69**, 148–160.

Dutton, J. A., 1976: *The Ceaseless Wind: An Introduction to the Theory of Atmospheric Motion.* McGraw-Hill, 579 pp.

Emanuel, K. A., 1979: Inertial instability and mesoscale convective systems. Part I: Linear theory of inertial instability in rotating viscous fluid. *J. Atmos. Sci.*, **36**, 2425–2449.

——, 1983a: On assessing local conditional symmetric instability from atmospheric soundings. *Mon. Wea. Rev.*, **111**, 2016–2033.

——, 1983b: The Lagrangian parcel dynamics of moist symmetric instability. *J. Atmos. Sci.*, **40**, 2368–2376.

——, 1988: Observational evidence of slantwise convective adjustment. *Mon. Wea. Rev.*, **116**, 1805–1816.

Fritsch, J. M., and C. F. Chappell, 1980: Numerical prediction of convectively driven mesoscale pressure systems. Part I: Convective parameterization. *J. Atmos. Sci.*, **37**, 1722–1733.

——, and R. A. Maddox, 1981: Convectively driven mesoscale weather systems aloft. Part I: Observations. *J. Appl. Meteor.*, **20**, 9–19.

——, and J. M. Brown, 1982: On the generation of convectively driven mesohighs aloft. *Mon. Wea. Rev.*, **110**, 1554–1563.

Gallus, W. A., Jr., and R. H. Johnson, 1991: Heat and moisture budgets of an intense midlatitude squall line. *J. Atmos. Sci.*, **48**, 122–146.

——, and ——, 1992: The momentum budget of an intense midlatitude squall line. *J. Atmos. Sci.*, **49**, 422–450.

Gao, K., D.-L. Zhang, M. W. Moncrieff, and H.-R. Cho, 1990: Mesoscale momentum budget in a midlatitude squall line: A numerical case study. *Mon. Wea. Rev.*, **118**, 1011–1028.

Hadlock, R., and C. W. Kreitzberg, 1988: The Experiment on Rapidly Intensifying Cyclones over the Atlantic (ERICA) field study: Objectives and plans. *Bull. Amer. Meteor. Soc.*, **69**, 1309–1320.

Hoskins, B. J., 1974: The role of potential vorticity in symmetric stability and instability. *Quart. J. Roy. Meteor. Soc.*, **100**, 480–482.

Houze, R. A., Jr., 1977: Structure and dynamics of a tropical squall-line system. *Mon. Wea. Rev.*, **105**, 1540–1567.

——, S. A. Rutledge, M. I. Biggerstaff, and B. F. Smull, 1989: Interpretation of Doppler weather radar displays of midlatitude mesoscale convective systems. *Bull. Amer. Meteor. Soc.*, **70**, 608–619.

——, B. F. Smull, and P. Dodge, 1990: Mesoscale organization of springtime rainstorms on Oklahoma. *Mon. Wea. Rev.*, **118**, 613–654.

Huschke, R. E., 1959: *Glossary of Meteorology.* Amer. Meteor. Soc., 638 pp.

Johnson, R. H., and P. J. Hamilton, 1988: The relationship of surface pressure features to the precipitation and air flow structure of an intense midlatitude squall line. *Mon. Wea. Rev.*, **116**, 1444–1472.

——, S. Chen, G. J. Stumpf, and D. L. Bartels, 1990: The vertical structure of a midtropospheric vortex within the stratiform region of a mesoscale convective system. *Extended Abstract, Fourth Conf. on Mesoscale Processes,* Amer. Meteor. Soc., 216–217.

Kasahara, A., 1982: Significance of non-elliptic regions in balanced flows of the tropical atmosphere. *Mon. Wea. Rev.*, **110**, 1956–1967.

Keyser, D., and R. Rotunno, 1990: On the formation of potential-vorticity anomalies in upper-level jet–front systems. *Mon. Wea. Rev.*, **118**, 1914–1921.

Knight, D. J., and P. V. Hobbs, 1988: The mesoscale and microscale structure and organization of clouds and precipitation in midlatitude cyclones. Part XV: A numerical modeling study of frontogenesis and cold-frontal rainbands. *J. Atmos. Sci.*, **45**, 915–930.

Kuettner, J. P., and D. E. Parker, 1976: GATE: Report on the field phase. *Bull. Amer. Meteor. Soc.*, **57**, 11–30.

Kuo, Y.-H., and R. A. Anthes, 1984: Mesoscale budgets of heat and moisture in a convective system over the central United States. *Mon. Wea. Rev.*, **112**, 1482–1497.

——, L. Cheng, and J.-W. Bao, 1988: Numerical simulation of the 1981 Sichuan flood. Part I: Evolution of a mesoscale southwest vortex. *Mon. Wea. Rev.*, **116**, 2481–2504.

Leary, C. A., and E. N. Rappaport, 1987: The life cycle and internal structure of a mesoscale convective complex. *Mon. Wea. Rev.*, **115**, 1503–1527.

McNab, A. L., and A. K. Betts, 1978: A mesoscale budget study of cumulus convection. *Mon. Wea. Rev.*, **106**, 1317–1331.

Menard, R. D., and J. M. Fritsch, 1989: A mesoscale convective complex-generated inertially stable warm core vortex. *Mon. Wea. Rev.*, **117**, 1237–1261.

Newton, C. W., 1950: Structure and mechanisms of the prefrontal squall line. *J. Meteor.*, **7**, 210–222.

Ogura, Y., and M.-T. Liou, 1980: The structure of a midlatitude squall line: A case study. *J. Atmos. Sci.*, **37**, 553–567.

Parsons, D. B., and P. V. Hobbs, 1983: The mesoscale and microscale structure and organization of clouds and precipitation in midlatitude cyclones. XI: Comparisons between observational and theoretical aspects of rainbands. *J. Atmos. Sci.*, **40**, 2377–2397.

Pedgley, D. E., 1962: A meso-synoptic analysis of the thunderstorms

on 28 August 1958. British Meteorological Office, Geophys. Memo, 106, 74 pp.

Persson, O. G., and T. T. Warner, 1991: Model generation of spurious gravity waves due to inconsistency of the vertical and horizontal resolution. *Mon. Wea. Rev.*, **119**, 917–935.

Raymond, D. J., and H. Jiang, 1990: A theory for long-lived mesoscale convective systems. *J. Atmos. Sci.*, **47**, 3067–3077.

Reuter, G. W., and M. K. Yau, 1990: Observations of slantwise convective instability in winter cyclones. *Mon. Wea. Rev.*, **118**, 447–458.

Rutledge, S. A., and R. A. Houze, Jr., 1987: A diagnostic modeling study of the trailing stratiform region of a midlatitude squall line. *J. Atmos. Sci.*, **44**, 2640–2656.

——, ——, M. I. Biggerstaff, and T. Matejka, 1988: The Oklahoma–Kansas mesoscale convective system of 10–11 June 1985: Precipitation structure and single-Doppler radar analysis. *Mon. Wea. Rev.*, **116**, 1409–1430.

Shapiro, M. A., 1976: The role of turbulent heat flux in the generation of potential vorticity in the vicinity of upper-level jet stream systems. *Mon. Wea. Rev.*, **104**, 892–906.

——, E. G. Donall, P. J. Neiman, L. S. Fedor, and N. González, 1991: Recent refinements in the conceptual models of extratropical cyclones. Preprints, *First Int. Symp. Winter Storms*, New Orleans, Amer. Meteor. Soc., 6–14.

Smull, B. F., and R. A. Houze, Jr., 1985: A midlatitude squall line with a trailing region of stratiform rain: Radar and satellite observations. *Mon. Wea. Rev.*, **113**, 117–133.

——, and ——, 1987: Rear inflow in squall lines with trailing stratiform precipitation. *Mon. Wea. Rev.*, **115**, 2869–2889.

Thorpe, A. J., M. J. Miller, and M. W. Moncrieff, 1982: Two-dimensional convection in nonconstant shear. A model of midlatitude squall lines. *Quart. J. Roy. Meteor. Soc.*, **108**, 739–762.

Xu, Q., 1986: Conditional symmetric instability and mesoscale rainbands. *Quart. J. Roy. Meteor. Soc.*, **112**, 315–334.

Zhang, D.-L., and J. M. Fritsch, 1987: Numerical simulation of the meso-β scale structure and evolution of the 1977 Johnstown flood. Part II: Inertially stable warm-core vortex and the mesoscale convective complex. *J. Atmos. Sci.*, **44**, 2593–2612.

——, and ——, 1988a: Numerical sensitivity experiments of varying model physics on the structure, evolution and dynamics of two mesoscale convective systems. *J. Atmos. Sci.*, **45**, 261–293.

——, and ——, 1988b: A numerical investigation of a convectively generated, inertially stable, extratropical warm-core mesovortex over land. Part I: Structure and Evolution. *Mon. Wea. Rev.*, **116**, 2660–2687.

——, and K. Gao, 1989: Numerical simulation of an intense squall line during 10–11 June 1985 PRE-STORM. Part II: Rear inflow, surface pressure perturbations and stratiform precipitation. *Mon. Wea. Rev.*, **117**, 2067–2094.

——, E.-Y. Hsie, and M. W. Moncrieff, 1988: A comparison of explicit and implicit predictions of convective and stratiform precipitating weather systems with a meso-β-scale numerical model. *Quart. J. Roy. Meteor. Soc.*, **114**, 31–60.

——, K. Gao, and D. B. Parsons, 1989: Numerical simulation of an intense squall line during 10–11 June 1985 PRE-STORM. Part I: Model verification. *Mon. Wea. Rev.*, **117**, 960–994.

Zipser, E. J., 1969: The role of organized unsaturated convective downdrafts in the structure and rapid decay of an equatorial disturbance. *J. Appl. Meteor.*, **8**, 799–814.

——, 1977: Mesoscale and convective-scale downdrafts as distinct components of squall-line structure. *Mon. Wea. Rev.*, **105**, 1568–1589.

——, R. J. Meitín, and M. A. LeMone, 1981: Mesoscale motion fields associated with a slowly moving GATE convective band. *J. Atmos. Sci.*, **38**, 1725–1750.